References

[1] H. Kroemer, "The physical principles of a negative-mass amplifier," *Proc. IRE*, vol. 47, pp. 397–406, March 1959.
[2] D. Pines and J. R. Schrieffer, "Collective behavior in solid-state plasmas," *Phys. Rev.*, vol. 124, pp. 1387–1400, December 1961.
[3] M. J. Harrison, "Collective excitation of degenerate plasmas in solids," *J. Phys. Chem. Solids*, vol. 23, pp. 1079–1086, August 1962.
[4] J. Dawson and C. Oberman, "Effect of ion correlations on high-frequency plasma conductivity," *Phys. of Fluids*, vol. 6, pp. 394–397, March 1963.
[5] E. Conwell, V. Fowler, and J. Zucker, unpublished.
[6] R. D. Larrabee, "Microwave impedance of semiconductor posts in waveguides, part I," *J. Appl. Phys.*, pp. 36, pp. 1597–1602, May 1965.
[7] G. Dousmanis, R. C. Duncan, J. J. Thomas and R. C. Williams, "Experimental evidence for carriers with negative mass," *Phys. Rev. (Letters)*, vol. 1, pp. 404–407, December 1958.
[8] F. Seifert, "Electrodeless microwave measurements of semiconductor resistivity and Faraday effect by cavity wall replacement," *Proc. IEEE (correspondence)*, vol. 53, pp. 752–753, July 1965.
[9] G. L. Allerton and J. R. Seifert, "Resistivity measurements of semiconductors at 9000 Mc," *IRE Trans. on Instrumentation*, vol. 9, pp. 175–179, September 1960.
[10] S. J. Buchsbaum and G. E. Smith, "Microwave induced D-C voltage in bismuth," *Phys. Rev. (Letters)*, vol. 9, pp. 342–343, October 1962.
[11] K. Rose, "Microwave induced carrier multiplication in indium antimonide," *J. Appl. Phys.*, vol. 33, pp. 761–762, February 1962.
[12] R. D. Larrabee, D. W. Woodard and W. A. Hicinbothem, Jr., "A two position probe method of microwave impedance measurements for the determination of the electrical properties of indium antimonide, pt. II," *J. Appl. Phys.*, vol. 36, pp. 1659–1663, May 1965.
[13] J. G. Linhart, I. M. Templeton, and R. Dunsmuir, "A microwave resonant cavity method for measuring the resistivity of semiconducting materials," *Brit. J. of Appl. Phys.*, vol. 7, pp. 36–38, January 1956.
[14] T. S. Benedict and W. Shockley, "Microwave observation of collision frequency of electrons in germanium," *Phys. Rev.*, vol. 89, pp. 1152–1153, March 1953.
[15] S. Roberts and A. Von Hippel, "A new method for measuring dielectric constant and loss in the range of centimeter waves," *J. Appl. Phys.*, vol. 17, pp. 610–616, July 1946.
[16] K. S. Champlin and R. R. Krongard, "The measurement of conductivity and permittivity of semiconductor spheres by an extension of the cavity perturbation method," IRE Trans. on Microwave Theory and Technique, vol. MTT-9 pp. 545–551, November 1961.
[17] N. Marcuvitz, *Waveguide Handbook*. New York: McGraw-Hill, 1960, pp. 257–267.
[18] *Selected Constants Relative to Semiconductors*. P. Aigrain, Ed. New York: Pergamon, 1961.

A Technique for Measuring Individual Modes Propagating in Overmoded Waveguide

D. S. LEVINSON, MEMBER, IEEE, AND I. RUBINSTEIN, MEMBER, IEEE

Abstract—**A practical measurement technique for determining the relative amplitude and phase of the individual modes propagating in overmoded waveguide is described. A phase-sensitive detector is used to measure the output of fixed probes placed around a single transverse plane in a section of enlarged waveguide. The detected output is directly proportional to the modal components, and data reduction is performed manually. The use of oversize waveguide provides increased accuracy and permits total multimode power measurements in conjunction with mode analysis. The technique can be used for mode measurements up to the fourth harmonic in standard rectangular waveguide. Experiments described in the paper use a single frequency source. However, signal sources with spurious content can be evaluated using appropriate tunable RF band-pass filters.**

Introduction

MEASUREMENTS in waveguide containing two or more propagating modes has received considerable attention from microwave engineers in recent years. This paper describes a practical technique for mode measurement that can provide rapid performance data on waveguide components subjected to overmoded propagation of power.

An effective device or technique for measuring multimode power must be able to determine the power in each mode or measure the total power regardless of the number of modes present. Both approaches have been used by various independent investigators to measure multimode power, and a number of techniques have been developed for use with rectangular waveguide [1]–[6]. Of particular interest here is the technique reported by Taub, based on the use of an enlarged section of waveguide [1]. This technique measures the total multimode power in the waveguide without identification of, or regard for, the individual propagating modes.

This paper describes a simple and practical measurement technique for identifying the individual modes and determining their relative amplitude and phase using the same oversize waveguide as Taub. Whereas Taub's method requires enlarged waveguide as a basic component, its use for mode measurements proves to be advantageous from practical considerations rather than being required by theoretical considerations.

Manuscript received December 20, 1965; revised April 5, 1966.
The authors are with the Department of Applied Electronics, Airborne Instruments Laboratory, Deer Park, N. Y.

Some of the methods previously referred to for measuring total multimode power do obtain, in effect, the power in each mode. These include the methods of Forrer [2], Lewis [3], and Price [4]. Another method for determining the modal content is presented by Klinger [7].

Forrer used a moving-probe assembly to measure the amplitude and phase of the electric field at the walls of a standard-size rectangular waveguide. Using computer techniques to perform a Fourier analysis of the measured data, the power contained in each propagating mode was calculated. Although the method is theoretically sound, computer data reduction is considered impractical in many applications. Also, the sliding probe inhibited the voltage breakdown level of the waveguide.

Lewis used a series of mode couplers that selectively coupled a given mode to its own output port. By calibrating the couplers it was possible to measure the power contained in each mode. The usefulness of this method, however, is limited to frequencies below which no more than five or six modes can propagate. Also, the couplers had a usable fractional bandwidth of only about ten percent.

Price's method is essentially the same as that used by Forrer except that the measured data is obtained using a series of fixed probes inserted through two walls of the waveguide. Although better high-power capabilities resulted, computer data reduction was still necessary. Also, the computer program enhances the probability of large errors even for small errors in the probe readings.

Klinger used a method that required the measurement of the variation in the input SWR as a function of the position of a short-circuiting piston in the multimode waveguide. The modes were identified by observing the shape and spacing of the absorption resonances. This method assumes that the modes other than the fundamental mode are relatively small in amplitude. This assumption plus the requirement for a short-circuit termination restricts its use to a few select types of measurements.

With the mode measurement technique described here, sufficient data is obtained at a single cross section of the oversize waveguide (by sampling the fields at all four walls) to determine all modes up to the TE_{22} mode. This permits measurements from the fundamental to the upper portion of the third harmonic region. By applying practical considerations, this range can be extended to the fourth harmonic region.

Single-plane measurements are made possible using a phase-sensitive detector whose output is directly proportional to the sampled field amplitude multiplied by a relative phase factor. This eliminates the requirement for an independent phase measurement and a possible source of error.

When the relationships between the mode components and the phase-sensitive detector output voltages have been compiled for any particular measurement, the final data reduction to which the measured values are applied involves only algebraic addition. Depending on the number of possible propagating modes, the data reduction for first-order mode determinations can be accomplished manually in 10 to 20 minutes. First-order determinations yield the relative amplitude and phase of each mode without distinguishing between TE and TM modes. When it is necessary to separate these degenerate modes (second-order mode determination), relatively little additional data processing is required using the original data. The functional relationships between the measured data and the mode components are derived by considering only the total number of propagating modes. These can then be used with measurements performed in any size waveguide at the appropriate frequency.

Since the phase-sensitive detector is a balanced device, its dynamic range is limited by practical considerations to slightly better than 20 dB. This results in some amplitude value being computed for all possible propagating modes even though no energy is contained in some modes. With a well-balanced detector, however, the apparent measured amplitude of nonpropagating modes will be at least 20 dB below the highest propagating mode amplitude determined. When using this technique, it is the practice to discard those modes as nonpropagating whose amplitudes fall below the 20-dB limit. By this procedure individual mode amplitudes can be determined with accuracies better than ± 0.5 dB.

The use of oversize waveguide for the probe section provides a number of advantages. First, all modes propagate at about the same phase velocity as opposed to the dispersive property of standard-size waveguide. This considerably reduces the fabrication problems associated with probe alignment and increases the inherent accuracy of the measurements. Also, as shown in Levinson and Worontzoff [8], the oversize probe section does not degrade the power handling capability of the standard-size waveguide system being measured.

An obvious feature of using enlarged waveguide is that total multimode power measurements can be performed along with individual mode measurements. This feature made it possible to check the accuracy of the mode measurement method to account for total power by summing the power in each mode. In all cases, the summation of the modal powers agreed with the total measured power by better than ± 1.5 dB.

The instrumentation described for mode measurements is compatible only with CW signal sources, either single frequency (signal generator) or containing spurious outputs. With the latter appropriate filters must be used as shown in Fig. 1.

This paper presents the theoretical basis for the technique as well as examples and results of experimental

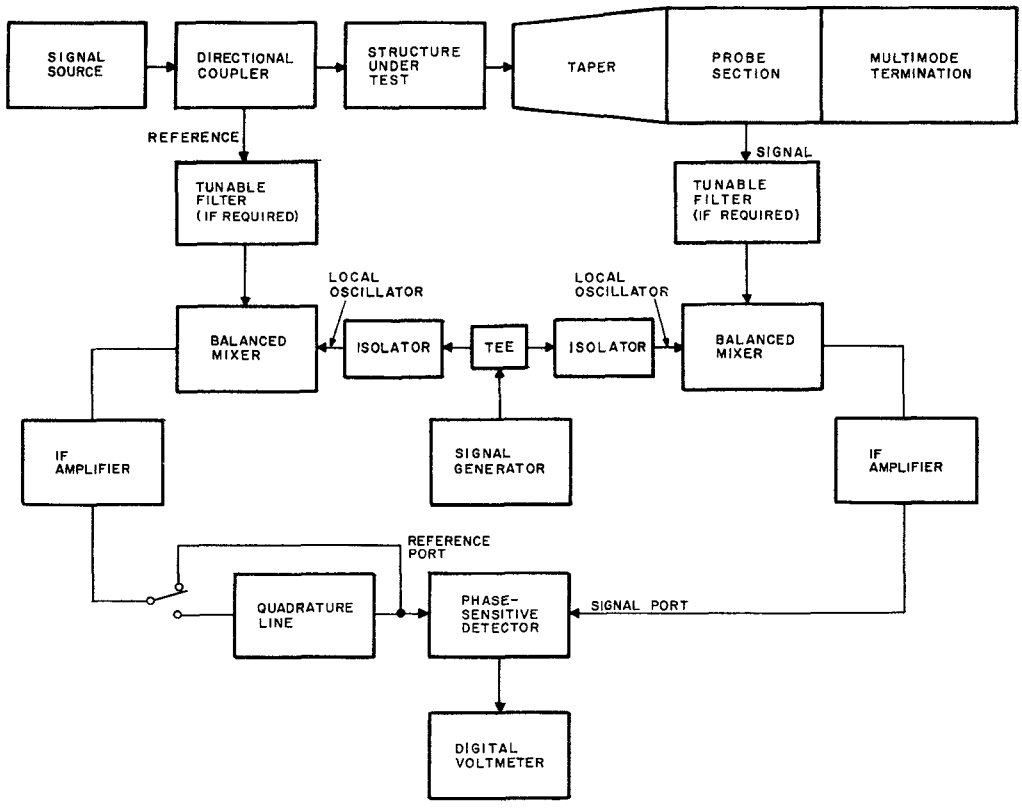

Fig. 1. Mode measurement setup.

work. A sample computation table is also derived to illustrate practical use of the theory when applied to a specific measurement. Second-order mode determinations are discussed and an example is presented.

Mode Measurements

Mode measurements are performed using the equipment shown in Fig. 1. The taper, probe section, and load are discussed in detail in Hinckelmann et al. [9]. Except for the phase-sensitive detector, the remaining components are standard laboratory equipment. A directional coupler is shown used in this setup to supply the reference signal, but a reference probe could be used as was done by Price [4]. The use of a single local oscillator source for both the reference and signal mixers ensures relative phase coherency without placing stringent stability requirements on the equipment.

A schematic diagram of the phase-sensitive detector is shown in Fig. 2. The theory and design parameters of the detector are described in Krishnan [11]. The operation of the detector can be outlined briefly as follows.

With a reference signal $V_R \angle \phi_r$ and a signal $V_S \angle \phi_s$ fed into their respective ports in the detector, the output voltage is given by

$$V_{\text{out}} = |V_S| \cos(\phi_s - \phi_r) \tag{1}$$

providing that $|V_R| > |V_S|$.

In the actual measurement setup, the reference signal is maintained at a minimum level of 6 dB above the strongest signal being sampled.

Since we are only concerned with relative phase data, the reference phase can be arbitrarily chosen so that $\phi_r = 0$. The output of the detector is then written simply as

$$V_{\text{out}} = |V_S| \cos \phi_s. \tag{2}$$

Using the quadrature line shown in Fig. 1, the detector can be used to obtain data with a quadrature phase relationship to the output given by (2). By switching to this line, an additional quarter wavelength is inserted in the reference arm of the detector so that the output relative to (2) is given by

$$V_{\text{out}} = |V_S| \cos\left(\phi_s - \frac{\pi}{2}\right) = |V_S| \sin \phi_s. \tag{3}$$

The detector output recorded with the line bypassed is arbitrarily termed the "in-phase" value; the output recorded with the line inserted is termed the "quadrature" value. These two measurements at each probe constitute the required measured data. The number of probes required is determined by the highest mode index being considered. Generally, m probes are required on each broad wall and n probes on each narrow wall. The

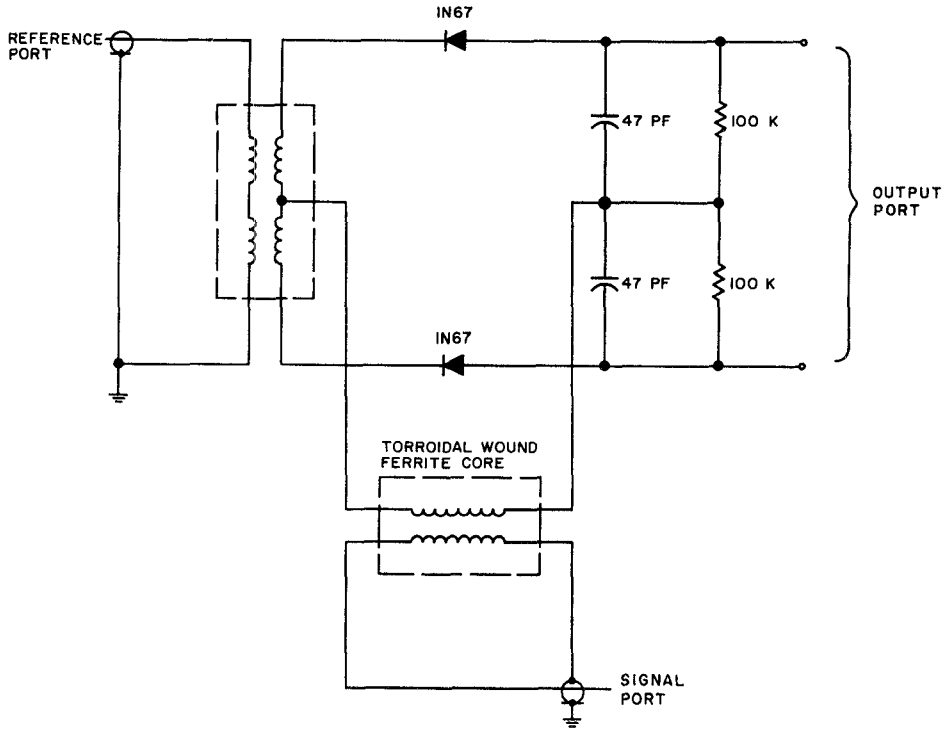

Fig. 2. Phase-sensitive detector.

output from the detector is read on a digital voltmeter used in the floating ground mode, and the sign of the output voltage is recorded along with its magnitude.

The measurement setup can be checked for balance and accuracy by performing a mode measurement at a frequency where only the dominant mode can propagate while assuming the presence of two modes. The resultant amplitude value of the known nonpropagating mode is a direct measure of the system accuracy. In a satisfactory setup, this value should be at least 20 dB down from the amplitude of the dominant mode.

Experimental Results

All mode measurements were performed on *S*-band components (WR-284) at a signal frequency of about 7.0 GHz. The first test conducted was a check of the mode conversion that takes place due to the tapers, which would be used on all subsequent tests. Figure 3 shows the waveguide components comprising the system to be tested.

In this setup, energy was launched into the system using the appropriate waveguide-to-coax adapter for the desired signal frequency. One taper was used to mate the adapter to a straight piece of *S*-band waveguide, and a second taper was used to mate with the oversize probe section. In later tests, the component whose mode conversion properties were to be tested replaced the straight section of waveguide.

Since the transition was excited in-band, a dominant mode would be launched, and any measured mode conversion would be the result of the tapers or flange misalignment. The results of mode measurements in this system are shown in Fig. 4. All the relative mode amplitudes computed are shown. When the 20-dB limit is applied and all modes below this level discarded as nonpropagating, only the dominant mode exists. Without any adjustments in the calibrations due to discarding the other modes, the total power is accounted for to within 3.4 percent of its true value. Thus, a measure of the accuracy of the system is obtained.

With this setup a dominant mode can be launched incident on any device inserted in place of the straight section. Any modes generated will be due to only the device being tested.

An inductive iris was fabricated (Fig. 5) and inserted in the line. With an incident dominant mode, Fig. 6 shows the measured mode conversion for this device. Note that the principal higher-order mode is the TE_{20}. The propensity for this device to convert an incident TE_{10} mode into the TE_{20} mode is predicted qualitatively by Southworth [12].

A standard 90-degree *E*-plane bend was inserted in the line, and the results of mode conversion to an incident dominant mode are shown in Fig. 7. Note that 74 percent of the power was converted into the TM_{11} mode, with only 19 percent of the power remaining in the dominant mode. The fact that this device favors propagation in the TM_{11} mode at out-of-band frequencies has been observed previously by other investigators [13].

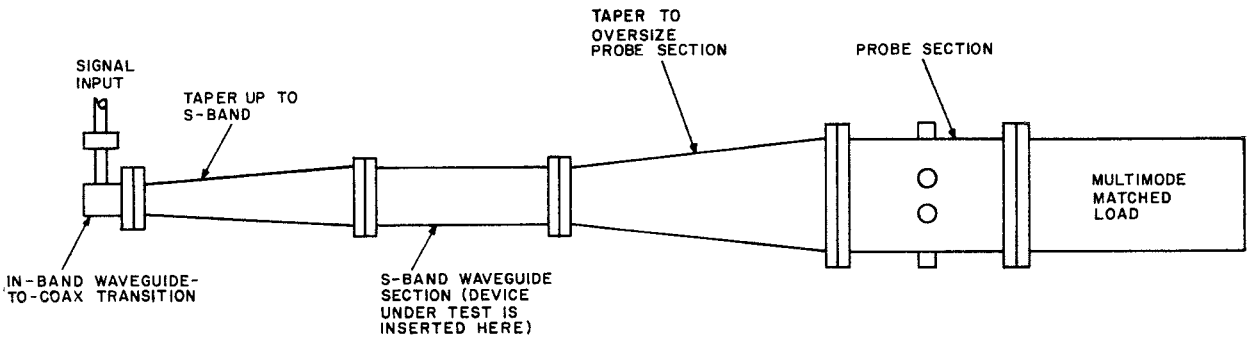

Fig. 3. Taper test setup.

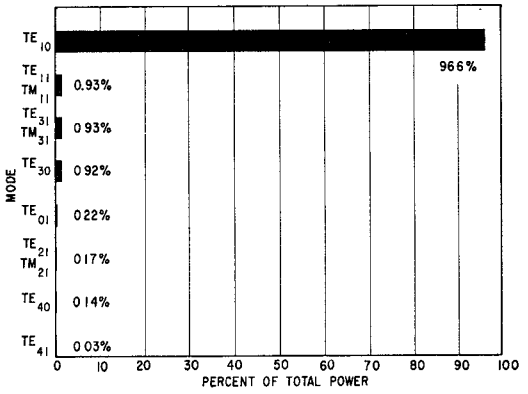

Fig. 4. Mode conversion due to tapers.

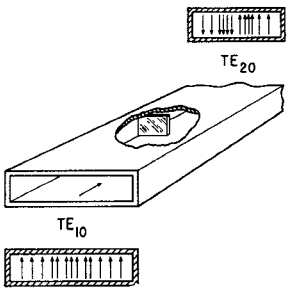

Fig. 5. Asymmetric inductive iris.

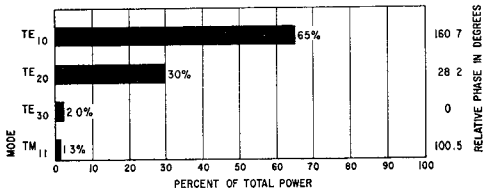

Fig. 6. Mode conversion for inductive iris.

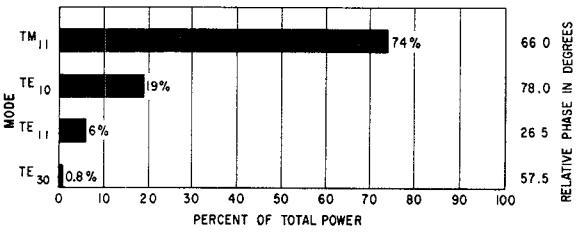

Fig. 7. Mode conversion for 90-degree E-plane bend.

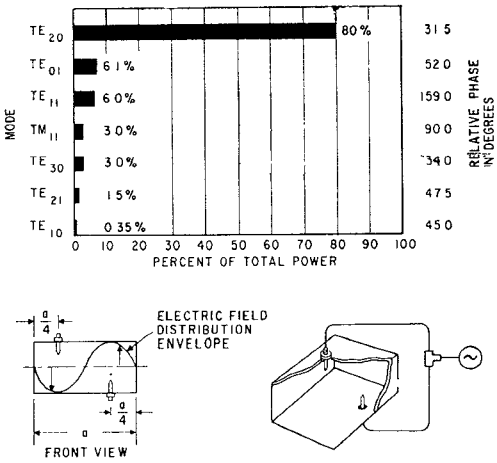

Fig. 8. TE_{20} mode launcher and measured performance.

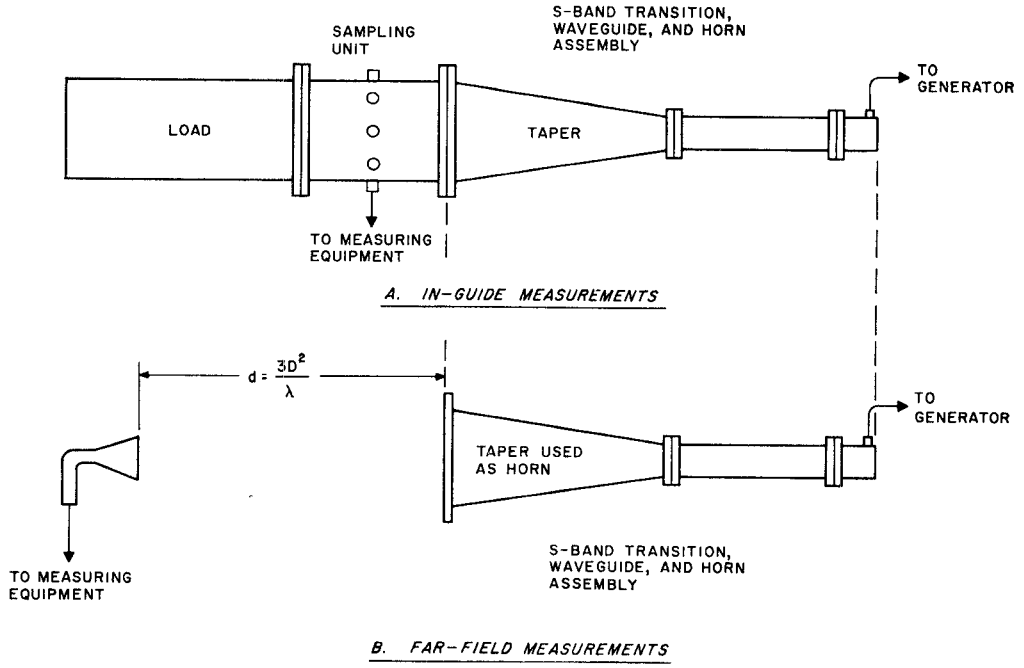

Fig. 9. *S*-band transition test and modified radiating system.

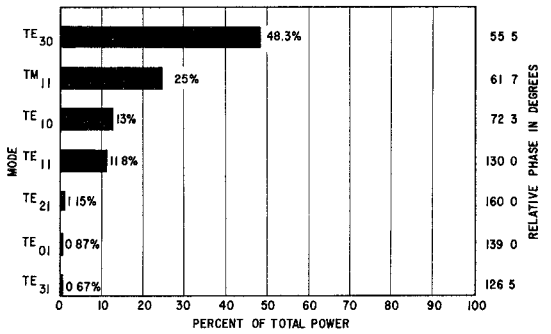

Fig. 10. Modes launched by *S*-band transition at $f=7.07$ MHz.

The ability to use the mode measurement technique to check the performance of devices designed to support or suppress certain modes was demonstrated by measuring the output of a TE_{20} mode launcher (Fig. 8). The measured output is shown in the same figure. This launcher is a fairly good device with 80 percent of the propagating energy being contained in the TE_{20} mode.

A standard *S*-band transition was connected directly to the straight section of *S*-band waveguide (Fig. 9A) and excited at a test frequency of 7.07 GHz. For this device, an exact theoretical analysis was performed of the primary mode conversion to be expected using methods outlined by Felsen [14]. The analysis indicated that the TE_{30} mode would be favored and that its amplitude relative to the TE_{10} mode would be greater by about 8 dB. Figure 10 shows that the TE_{30} mode amplitude does in fact exceed that of the dominant mode by about 6 dB.

Figure 9B shows the setup used in the previous test with the probe section and load removed. The remaining system then becomes a radiating system with the taper being used as a horn antenna. The mode measurements obtained in the previous test were translated from the plane of the probes to the plane of the taper to describe its overmoded aperture illumination. This data was then applied to farfield primary pattern prediction techniques described in Levinson [10], and the radiation pattern was sketched.

The actual radiated pattern from the system was then measured in the far field for the horn at the test frequency. The measured pattern is shown compared with the predicted pattern in Fig. 11. The two patterns agree to within one degree in angle at the nulls, and to within 3 dB in relative amplitude at the peaks of the main lobes.

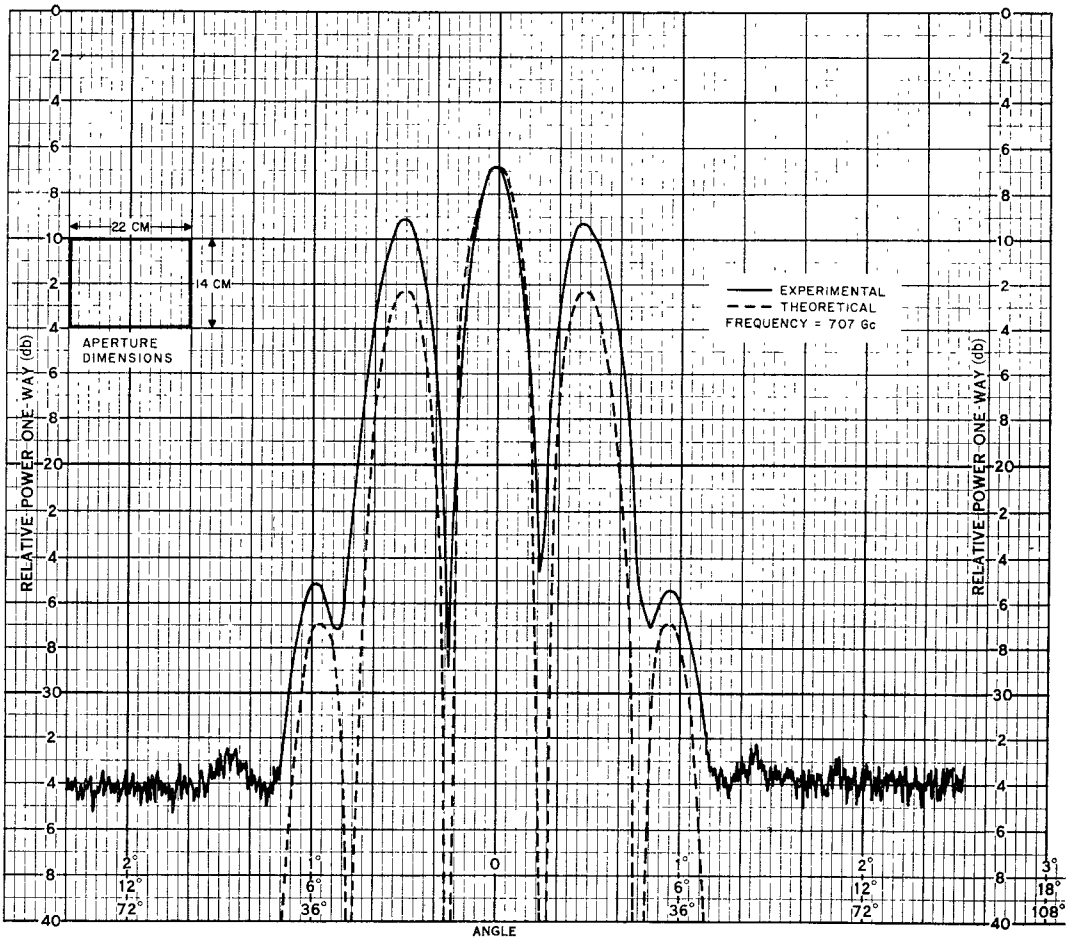

Fig. 11. Comparison of predicted and experimental far-field patterns of multimode aperture.

Theoretical Considerations

This portion of the theory outlines the basic detection scheme using the phase-sensitive detector. Other considerations in applying the theory to actual measurements are treated in the next section.

RF Output from Electric Field Probe in Overmoded Guide

Figure 12 shows a typical probe section that can be used for both mode measurements or total power measurements. Standard coordinates are used to describe the position of each wall, and the transverse measurement plane is taken at $z=0$ along the waveguide.

From standard waveguide theory, the electric fields in the guide perpendicular to the broad and narrow walls can be written for any number of modes as follows:

$$\overline{E}_y = \sum_{m=1}^{m}\sum_{n=0}^{n}\left(A_{mn}\sin\frac{m\pi x}{a}\cos\frac{n\pi y}{b}\right)\cdot\exp^{-j(\omega t+\beta_{mn}z+\theta_{mn})} \tag{4}$$

$$\overline{E}_x = \sum_{m=0}^{m}\sum_{n=1}^{n}\left(B_{mn}\sin\frac{n\pi y}{b}\cos\frac{m\pi x}{a}\right)\cdot\exp^{-j(\omega t+\beta_{mn}z+\theta_{mn})}. \tag{5}$$

The RF output from a probe placed along the broad wall in the $y=0$ plane is written from (1) by setting y and $z=0$, and $x=x_1$ to denote the actual probe position between the walls $x=0$ and $x=a$. The RF frequency (ωt) can be combined with θ_{mn} in the following discussion since it is a constant for all the modes. With these considerations, the probe output is given by

$$\overline{E}_y\big|_{x_1} = \sum_{m=1}^{m}\sum_{n=0}^{n}\left(A_{mn}\sin\frac{m\pi x_1}{a}\right)\exp^{j\theta_{mn}}. \tag{6}$$

To simplify the notation, let the quantity

$$\sin\frac{m\pi x_P}{a} = {}_mS_P. \tag{7}$$

This term is a constant multiplier for each mode once the actual probe position is selected.

By expanding (6) around $m=1, 2, 3, \cdots$, and regrouping, the probe output is written in the more convenient form:

$$\overline{E}_y\big|_{x_1} = {}_1S_1\sum_{n=0}^{n}A_{1n}\exp^{j\theta_{1n}} + {}_2S_1\sum_{n=0}^{n}A_{2n}\exp^{j\theta_{2n}} + \cdots + {}_mS_1\sum_{n=0}^{n}A_{mn}\exp^{j\theta_{mn}}. \tag{8}$$

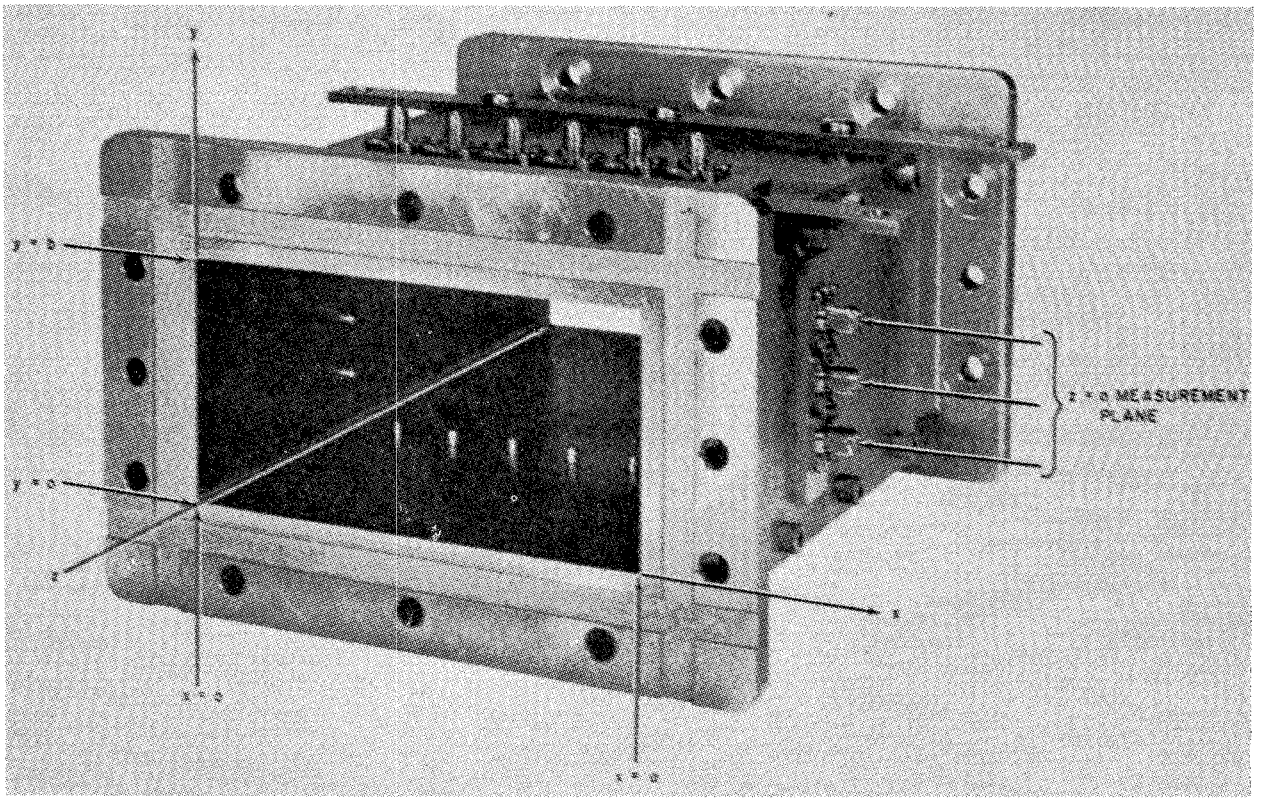

Fig. 12. Typical probe section with coordinate system.

Since the probe output is a vector quantity, it can be expressed in terms of its real and imaginary components as follows:

$$\begin{aligned}\overline{E}_y\big|_{x_1} &= \left|\overline{E}_y\big|_{x_1}\right| (\cos\psi + j\sin\psi) \\ &= \operatorname{Re}(\overline{E}_y\big|_{x_1}) + j\operatorname{Im}(\overline{E}_y\big|_{x_1}) \end{aligned} \tag{9}$$

where

$$\operatorname{Re}(\overline{E}_y\big|_{x_1}) = {}_1S_1\sum_{n=0}^{n} A_{1n}\cos\theta_{1n} + {}_2S_1\sum_{n=0}^{n} A_{2n}\cos\theta_{2n} + \cdots + {}_mS_1\sum_{n=0}^{n} A_{mn}\cos\theta_{mn} \tag{10}$$

$$\operatorname{Im}(\overline{E}_y\big|_{x_1}) = {}_1S_1\sum_{n=0}^{n} A_{1n}\sin\theta_{1n} + {}_2S_1\sum_{n=0}^{n} A_{2n}\sin\theta_{2n} + \cdots + {}_mS_1\sum_{n=0}^{n} A_{mn}\sin\theta_{mn}. \tag{11}$$

The RF output from a probe placed on a narrow wall of the waveguide is obtained in a similar manner.

If a standard amplitude detector (crystal, bolometer, etc.) were connected to the probe at $x=x_1$, the output would be a measure of the amplitude of $\overline{E}_y\big|_{x_1}$. The amplitude is obtained by forming the square root of the sum of the squares of the real and imaginary components given in (10) and (11). Without actually writing out this quantity, it can be seen that the amplitude will contain a number of cross-product terms depending on the number of modes. From data obtained at only a single cross section of the waveguide, the terms comprising the cross products are inseparable. It is evident, then, that a standard detector cannot be used with this mode measurement method.

Application of Phase-Sensitive Detection

When the phase-sensitive detector, previously described, is connected to the sampling probe located at $x=x_1$, the output of the detector is proportional to either the real or imaginary part of the sampled field as they are given in (9) and defined in (10) and (11). Both components, real and imaginary, are composed of a linear combination of the individual mode terms. Thus, the phase-sensitive detector yields a direct measure of this linear mode sum. By repeated measurements at other probes located in the same transverse plane, a system of linear simultaneous equations results. These can be solved for each mode term as a function of the phase-sensitive detector voltages. The following example illustrates this process.

Application of Theory (Simple Two-Mode Case)

Consider a simple case of mode measurements performed at a frequency where only two modes are capable of propagating in the waveguide. In standard rectangular waveguide, the first two modes are the TE_{10} and TE_{20}. The relationship between the modes and the phase-sensitive detector output voltages are derived as follows. From (10) and (11), the mode sums for this example become

$$\text{Re}\,(E_y|_{x_1}) = {}_1S_1A_{10}\cos\theta_{10} + {}_2S_1A_{20}\cos\theta_{20} = V_{I1} \quad (12)$$

$$\text{Im}\,(E_y|_{x_1}) = {}_1S_1A_{10}\sin\theta_{10} + {}_2S_1A_{20}\sin\theta_{20} = V_{Q1}. \quad (13)$$

These sums are shown equated to the "in-phase" and "quadrature" detector output voltages from measurements at probe 1. With measurements repeated at a second probe on the same broad wall of the waveguide, the following mode sums result:

$$\text{Re}\,(E_y|_{x_2}) = {}_1S_2A_{10}\cos\theta_{10} + {}_2S_2A_{20}\cos\theta_{20} = V_{I2} \quad (14)$$

$$\text{Im}\,(E_y|_{x_2}) = {}_1S_2A_{10}\sin\theta_{10} + {}_2S_2A_{20}\sin\theta_{20} = V_{Q2}. \quad (15)$$

Note that in these last expressions for the output at the second probe, only the constants ${}_mS_P$ have changed. These constants account for the transverse field distribution of the modes with which they are associated [see (7)].

By considering each mode amplitude times its phase factor as a single term, the four equations comprise a double set of linear simultaneous equations that are solved as follows:

$$A_{10}\cos\theta_{10} = f({}_mS_P, V_{I1}, V_{I2}) = M_{10} \quad (16)$$

$$A_{20}\cos\theta_{20} = g({}_mS_P, V_{I1}, V_{I2}) = M_{20} \quad (17)$$

$$A_{10}\sin\theta_{10} = f({}_mS_P, V_{Q1}, V_{Q2}) = N_{10} \quad (18)$$

$$A_{20}\sin\theta_{20} = g({}_mS_P, V_{Q1}, V_{Q2}) = N_{20}. \quad (19)$$

The relative amplitudes and phases of the two modes are then obtained as follows:

$$A_{10} = \sqrt{(M_{10})^2 + (N_{10})^2} \qquad \theta_{10} = \tan^{-1}\frac{N_{10}}{M_{10}} \quad (20)$$

$$A_{20} = \sqrt{(M_{20})^2 + (N_{20})^2} \qquad \theta_{20} = \tan^{-1}\frac{N_{20}}{M_{20}}. \quad (21)$$

Comments on Example

For simple cases of mode measurements, data from only one broad wall and one narrow wall (if required) are sufficient. This is true only when all the possible propagating modes have one mode index equal to zero. This condition is satisfied for the first three modes in both WR284 and WR650 waveguides. In general, data from all four walls are required. For any particular measurement, the number of probes on each broad and narrow wall is determined by the highest m and n mode index, respectively.

Computation Table

This section is concerned with deriving a typical computation table for use with mode measurements. The example is performed at the theoretical upper limit of this technique to illustrate the manner in which the limitation is imposed and to point out practical details that arise when deriving the mode component/output voltage relationships.

General Form of Mode-Sum Equations

For this example, assume that measurements are desired in S-band waveguide just at the cutoff frequency of the TE_{22} mode, 9.739 GHz. Although this mode can be ignored as nonpropagating, it will be included in the initial steps to illustrate the limiting properties of the technique.

In deriving this table, only the TE mode notation will be used and, where applicable, will represent the sum of a TE and TM mode. The separation of these modes is discussed in the next section.

The most useful way to represent the general mode-sum equations is in matrix form. For one broad wall, the matrix is given by

$$\begin{pmatrix} {}_1S_1 & {}_2S_1 & \cdots & {}_mS_1 \\ {}_1S_2 & {}_2S_2 & \cdots & {}_mS_2 \\ \vdots & \vdots & & \vdots \\ {}_1S_P & {}_2S_P & \cdots & {}_mS_P \\ \vdots & \vdots & & \vdots \\ {}_1S_m & {}_2S_m & \cdots & {}_mS_m \end{pmatrix} \begin{pmatrix} V_{(I,Q)1} \\ V_{(I,Q)2} \\ \vdots \\ V_{(I,Q)P} \\ \vdots \\ V_{(I,Q)m} \end{pmatrix} = \begin{pmatrix} V_{(I,Q)1} \\ V_{(I,Q)2} \\ \vdots \\ V_{(I,Q)P} \\ \vdots \\ V_{(I,Q)m} \end{pmatrix} \quad (22)$$

where

$${}_mS_P = \sin\frac{m\pi x_P}{a},$$

P = probe number 1, 2, 3 $\cdots$ m,

$V_{(I,Q)P}$ = detector voltage at probe P (in-phase or quadrature),

$$Y_{(I,Q)P} = \sum_{n=0}^{n} A_{Pn}\begin{pmatrix}\cos\\ \sin\end{pmatrix}\theta_{Pn}.$$

The matrix used for the opposite wall is identical to (22) except for 1) the definition of the summations given by Y, and 2) a minus sign preceding all measured voltages noted by V.

Using primes to denote values for the opposite wall, the sums are defined by

$$Y'_{(I,Q)P} = \sum_{n=0}^{n}(-1)^n A_{Pn}\begin{pmatrix}\cos\\ \sin\end{pmatrix}\theta_{Pn}. \quad (23)$$

The need to define the summations differently is due to the relative phase reversal of the electric field of certain modes between opposite walls. The E_y field component of modes with an odd n index experiences a phase reversal between opposite broad walls of the guide, and the E_x field component reverses its phase between the narrow walls for modes with an odd m index.

The minus sign preceding the measured voltage values for the opposite wall accounts for the physical inversion of the probes. In the actual measurements, it makes no difference which wall is noted—top or bottom or left or right—as long as a consistent reference is used.

For the narrow walls of the waveguide, a matrix similar to (22) is used as given below:

$$\begin{bmatrix} {}_1S_1 & {}_2S_1 \cdots {}_nS_1 \\ \vdots & \\ {}_1S_p & {}_2S_p \cdots {}_nS_p \\ \vdots & \\ {}_1S_n & {}_2S_n \cdots {}_nS_n \end{bmatrix} \begin{bmatrix} x_{(I,Q)1} \\ \vdots \\ x_{(I,Q)p} \\ \vdots \\ x_{(I,Q)n} \end{bmatrix} = \begin{bmatrix} v_{(I,Q)1} \\ \vdots \\ v_{(I,Q)p} \\ \vdots \\ v_{(I,Q)n} \end{bmatrix} \tag{24}$$

where

$${}_nS_p = \sin \frac{n\pi y_p}{b},$$

p = probe number 1, 2 $\cdots$ n,

$v_{(I,Q)p}$ = detector voltage at probe p (in-phase or quadrature),

$$x_{(I,Q)p} = \sum_{m=0}^{m} B_{mp} \begin{pmatrix} \cos \\ \sin \end{pmatrix} \theta_{mp}.$$

As with the opposite broad-wall matrix, the opposite narrow-wall matrix is identical to (24) except that a minus sign precedes the measured voltages noted by v, and the summation given by x is defined by

$$x'_{(I,Q)p} = \sum_{m=0}^{m} (-1)^m B_{mp} \begin{pmatrix} \cos \\ \sin \end{pmatrix} \theta_{mp}. \tag{25}$$

Probe Section

The highest mode indexes being considered in this example are $m=4$ and $n=2$. The probe section then will have four probes on each broad wall and two probes on each narrow wall of the waveguide. Assume that the probes are positioned as follows.

Along the broad walls:

$$P1 \text{ is positioned at } x_1 = \frac{a}{8}$$

$$P2 \text{ is positioned at } x_2 = \frac{3a}{8}$$

$$P3 \text{ is positioned at } x_3 = \frac{5a}{8}$$

$$P4 \text{ is positioned at } x_4 = \frac{7a}{8}.$$

Along the narrow walls:

$$p1 \text{ is positioned at } y_1 = \frac{b}{3}$$

$$p2 \text{ is positioned at } y_2 = \frac{2b}{3}.$$

Matrix Solutions

Using the values given for the probe positions in matrix equations (22) and (24), and the in-phase notation, the matrixes become

$$\begin{bmatrix} (\sqrt{2-\sqrt{2}}) & \left(\frac{\sqrt{2}}{2}\right) & (\sqrt{2+\sqrt{2}}) & (1) \\ (\sqrt{2+\sqrt{2}}) & \left(\frac{\sqrt{2}}{2}\right) & -(\sqrt{2-\sqrt{2}}) & (-1) \\ (\sqrt{2+\sqrt{2}}) & -\left(\frac{\sqrt{2}}{2}\right) & -(\sqrt{2-\sqrt{2}}) & (1) \\ (\sqrt{2-\sqrt{2}}) & -\left(\frac{\sqrt{2}}{2}\right) & (\sqrt{2+\sqrt{2}}) & (-1) \end{bmatrix} \begin{bmatrix} Y_{I1} \\ Y_{I2} \\ Y_{I3} \\ Y_{I4} \end{bmatrix}$$

$$= \begin{bmatrix} V_{I1} \\ V_{I2} \\ V_{I3} \\ V_{I4} \end{bmatrix} \tag{26}$$

$$\begin{bmatrix} \left(\frac{\sqrt{3}}{2}\right) & \left(\frac{\sqrt{3}}{2}\right) \\ \left(\frac{\sqrt{3}}{2}\right) & -\left(\frac{\sqrt{3}}{2}\right) \end{bmatrix} \begin{bmatrix} x_{I1} \\ x_{I2} \end{bmatrix} = \begin{bmatrix} v_{I1} \\ v_{I2} \end{bmatrix}. \tag{27}$$

Solving the above for Y and x, we get

$$Y_{I1} = \frac{1}{4}[\sqrt{2-\sqrt{2}}\,(V_{I1} + V_{I4}) + \sqrt{2+\sqrt{2}}\,(V_{I2} + V_{I3})] \tag{28}$$

$$Y_{I2} = \frac{1}{2\sqrt{2}}[V_{I1} + V_{I2} - V_{I3} - V_{I4}] \tag{29}$$

$$Y_{I3} = \frac{1}{4}[\sqrt{2+\sqrt{2}}\,(V_{I1} + V_{I4}) - \sqrt{2-\sqrt{2}}\,(V_{I2} + V_{I3})] \tag{30}$$

$$Y_{I4} = \frac{1}{4}[V_{I1} - V_{I2} + V_{I3} - V_{I4}] \tag{31}$$

$$x_{I1} = \frac{1}{\sqrt{3}}[v_{I1} + v_{I2}] \tag{32}$$

$$x_{I2} = \frac{1}{\sqrt{3}}[v_{I1} - v_{I2}]. \tag{33}$$

The solutions using quadrature measurements are obtained by merely changing the subscripts. Also, these same solutions hold when opposite wall data is used by changing the sign preceding each measured value noted by V and v.

Equations (28)–(33) represent the first entries in the computation table. It is seen that the values for Y and x are obtained by the algebraic addition of the detector output voltage at each probe.

Mode Sums and Separation

The next step in deriving the table is to form the relationships between the individual mode terms and the computed values of Y and x as given above. This is done by writing out the mode sums according to (22)–(25). This is done below for all four walls using the in-phase notation.

From (22):

$$Y_{I1} = A_{10}\cos\theta_{10} + A_{11}\cos\theta_{11} + A_{12}\cos\theta_{12} \quad (34)$$

$$Y_{I2} = A_{20}\cos\theta_{20} + A_{21}\cos\theta_{21} + (A_{22}\cos\theta_{22}) \quad (35)$$

$$Y_{I3} = A_{30}\cos\theta_{30} + A_{31}\cos\theta_{31} \quad (36)$$

$$Y_{I4} = A_{40}\cos\theta_{40} + A_{41}\cos\theta_{41}. \quad (37)$$

From (23):

$$Y_{I1}' = A_{10}\cos\theta_{10} - A_{11}\cos\theta_{11} + A_{12}\cos\theta_{12} \quad (38)$$

$$Y_{I2}' = A_{20}\cos\theta_{20} - A_{21}\cos\theta_{21} + (A_{22}\cos\theta_{22}) \quad (39)$$

$$Y_{I3}' = A_{30}\cos\theta_{30} - A_{31}\cos\theta_{31} \quad (40)$$

$$Y_{I4}' = A_{40}\cos\theta_{40} - A_{41}\cos\theta_{41}. \quad (41)$$

From (24):

$$x_{I1} = B_{01}\cos\theta_{01} + B_{11}\cos\theta_{11} + B_{21}\cos\theta_{21} + B_{31}\cos\theta_{31} + B_{41}\cos\theta_{41} \quad (42)$$

$$x_{I2} = B_{02}\cos\theta_{02} + B_{12}\cos\theta_{12} + (B_{22}\cos\theta_{22}). \quad (43)$$

From (25):

$$x_{I1}' = B_{01}\cos\theta_{01} - B_{11}\cos\theta_{11} + B_{21}\cos\theta_{21} - B_{31}\cos\theta_{31} + B_{41}\cos\theta_{41} \quad (44)$$

$$x_{I2}' = B_{02}\cos\theta_{02} - B_{12}\cos\theta_{12} + (B_{22}\cos\theta_{22}). \quad (45)$$

The method for separating each mode term is to combine the mode sum expressions for opposite walls. For example, by adding and subtracting (37) and (41), the TE_{40} and TE_{41} mode elements are separated. This process is repeated for all the sums until each mode element is separated.

For those sums containing more than two terms, the fixed relationship between orthogonal field amplitudes for the same mode is used to effect the final separation. These are given by

$$\frac{A_{mn}}{B_{mn}} = \frac{mb}{na} \quad \text{for TE modes} \quad (46)$$

$$\frac{A_{mn}}{B_{mn}} = \frac{na}{mb} \quad \text{for TM modes.} \quad (47)$$

For the first-order mode determinations, (46) is used.

All the terms in the sums can be separated, using these considerations, but only if the TE_{22} mode is dropped from the equations. No amount of manipulation can cause this term to be expressed independently because in all the equations it appears as a third term. The method of separating the modes depends on the fact that each mode element appears either singly or in pairs in at least one set of equations. Thus, the mode measurement technique is limited to the determination of modes below the TE_{22}. If practical considerations determine that negligible energy is contained in modes with even n indexes, this term plus the TE_{32} and TE_{42} can be ignored. The technique can then be extended beyond the fourth harmonic region for mode determinations up to the TE_{13} mode. As the experimental data shows, the assumption for extending the frequency range is valid for most standard waveguide systems.

Final Mode Element Relationships

When all the mode elements are separated in the manner indicated, the following relationships result:

$$A_{10}\cos\theta_{10} = \frac{1}{2}(Y_{I1} + Y_{I1}') - \frac{b}{4a}(x_{I2} - x_{I2}') = M_{10}$$

$$A_{11}\cos\theta_{11} = \frac{1}{2}(Y_{I1} - Y_{I1}') = M_{11}$$

$$A_{20}\cos\theta_{20} = \frac{1}{2}(Y_{I2} + Y_{I2}') = M_{20}$$

$$A_{21}\cos\theta_{21} = \frac{1}{2}(Y_{I2} - Y_{I2}') = M_{21}$$

$$A_{30}\cos\theta_{30} = \frac{1}{2}(Y_{I3} + Y_{I3}') = M_{30}$$

$$A_{31}\cos\theta_{31} = \frac{1}{2}(Y_{I3} - Y_{I3}') = M_{31}$$

$$A_{40}\cos\theta_{40} = \frac{1}{2}(Y_{I4} + Y_{I4}') = M_{40}$$

$$A_{41}\cos\theta_{41} = \frac{1}{2}(Y_{I4} - Y_{I4}') = M_{41}$$

$$B_{01}\cos\theta_{01} = \frac{1}{2}(x_{I1} + x_{I1}') + \frac{b}{a}(Y_{I2} + Y_{I2}') + \frac{2b}{a}(Y_{I4} - Y_{I4}') = C_{01}$$

$$B_{02}\cos\theta_{02} = \frac{1}{2}(x_{I2} + x_{I2}') = C_{02}$$

$$B_{12}\cos\theta_{12} = \frac{1}{2}(x_{I2} - x_{I2}') = C_{12}. \quad (48)$$

A similar set is compiled for the quadrature data by interchanging sine for cosine and the subscript Q for I. To indicate the notation, two terms in that set would be

$$A_{11} \sin \theta_{11} = \frac{1}{2}(Y_{Q1} - Y_{Q1}') = N_{11}$$

$$B_{02} \sin \theta_{02} = \frac{1}{2}(x_{Q2} + x_{Q2}') = D_{02}. \quad (49)$$

The relative amplitude and phase of each mode is then determined, as was done in (20) and (21), with the notation as shown below:

$$A_{mn} = \sqrt{(M_{mn})^2 + (N_{mn})^2} \qquad \theta_{mn} = \tan^{-1}\frac{N_{mn}}{M_{mn}} \quad (50)$$

$$B_{mn} = \sqrt{(C_{mn})^2 + (D_{mn})^2} \qquad \theta_{mn} = \tan^{-1}\frac{D_{mn}}{C_{mn}}. \quad (51)$$

Final Details of Table

Equations (48)–(51) complete the elements for the computation table. The following steps summarize the computation procedure.

1) Obtain measured in-phase and quadrature data at each probe on all four walls.
2) Solve (28)–(33) using the measured values.
3) Determine the value of each mode element according to (48) and (49) using the values obtained in step 2.
4) Calculate the relative amplitudes and phases of each of the modes as given by (50) and (51).

Example of Results from Mode Measurements

The following table shows the calculated mode amplitudes for first-order mode determinations using data obtained in an actual test at a signal frequency com patible with the table derived in the preceding example.

Mode Index	Calculated Amplitude (mV)	Relative Amplitude (dB)
*10	174.0	−6.0
20	19.5	−28.8
01	8.3	−37.3
*11	300.0	−1.2
21	14.0	−32.1
*30	347.0	0
*31	93.5	−11.4
40	18.0	−29.6
02	20.6	−28.2
12	6.6	−39.6
41	7.4	−38.4

By applying the 20-dB limit, it is seen that only four propagating modes exist (denoted by asterisks) and that the majority of the power is contained in the TE_{30} mode. Since a significant portion of the total power is contained in a mode which can exist in either or both the TE and TM modal configurations, the (TE, TM)$_{11}$, it might be desired to perform a second-order determination to obtain the amplitude of each mode. The method for doing this will be discussed in the next section.

Second-Order Mode Determination

The separation of TE and TM modes is similar to the method of separating the elements in the mode sums for first-order mode determination. This separation, second-order determination, is logically the final step in any mode measurement.

In general, all modes having one index equal to zero can exist only in the TE configuration, while modes having nonzero m and n indexes can exist in either the TE, TM, or both modal configurations simultaneously. When separation is desired, it is assumed that both modal configurations exist, and the following procedure is used to determine their relative amplitudes.

Separation Procedure for TE_{11} and TM_{11} Modes

Using the experimental results given, the appropriate expressions containing the (TE, TM)$_{11}$ mode in (34)-(45) are modified to indicate the existence of both types of modes.

$$Y_{I1} = A_{10}\cos\theta_{10} + (A_{TE_{11}}\cos\theta_{TE_{11}} - A_{TM_{11}}\cos\theta_{TM_{11}}) \quad (52)$$

$$Y_{I1}' = A_{10}\cos\theta_{10} - (A_{TE_{11}}\cos\theta_{TE_{11}} - A_{TM_{11}}\cos\theta_{TM_{11}}) \quad (53)$$

$$x_{I1} = (B_{TE_{11}}\cos\theta_{TE_{11}} + B_{TM_{11}}\cos\theta_{TM_{11}}) + B_{31}\cos\theta_{31} \quad (54)$$

$$x_{I1}' = -(B_{TE_{11}}\cos\theta_{TE_{11}} + B_{TM_{11}}\cos\theta_{TM_{11}}) - B_{31}\cos\theta_{31}. \quad (55)$$

In (52) and (53), the minus sign accounts for the antiphase property of the fields perpendicular to the broad walls for the two types of modes. The fields of the two types of modes perpendicular to the narrow walls are in-phase.

By combining pairs of equations as before, we get

$$A_{TE_{11}}\cos\theta_{TE_{11}} - A_{TM_{11}}\cos\theta_{TM_{11}} = M_{11} \quad (56)$$

$$B_{TE_{11}}\cos\theta_{TE_{11}} + B_{TM_{11}}\cos\theta_{TM_{11}} = \tfrac{1}{2}(x_{I1} - x_{I1}') - C_{31} = C_{11} \quad (57)$$

and from (46) and (48),

$$C_{31} = \left(\frac{a}{b}\right)\frac{M_{31}}{3}. \quad (58)$$

By using (46) and (47), the narrow-wall amplitudes of the two modes can be expressed in terms of the broad-wall amplitudes. Applying this to (57), we get

$$\left(\frac{a}{b}\right)A_{TE_{11}}\cos\theta_{TE_{11}} + \left(\frac{b}{a}\right)A_{TM_{11}}\cos\theta_{TM_{11}} = C_{11}. \quad (59)$$

Equations (56) and (59) are then solved to separate each of the modes.

$$A_{TE_{11}}\cos\theta_{TE_{11}} = \frac{1}{(a/b + b/a)}[C_{11} + (b/a)M_{11}] \quad (60)$$

$$A_{\mathrm{TM}_{11}} \cos \theta_{\mathrm{TM}_{11}} = \frac{1}{(a/b + b/a)} [C_{11} - (a/b)M_{11}]. \quad (61)$$

A similar set of equations can be written for use with the quadrature data from (60) and (61) by replacing the cosine with sine, C_{11} with D_{11}, and M_{11} with N_{11}.

$$D_{11} = \tfrac{1}{2}(x_{Q1} - x_{Q1}') - D_{31} \quad (62)$$

and

$$D_{31} = \left(\frac{a}{b}\right)\frac{N_{31}}{3}. \quad (63)$$

The individual mode amplitudes and phases are then obtained by the trigonometric identities, as was done before in (50) and (51), using the appropriate values calculated by the procedure outlined.

Conclusions

A practical technique for measuring the individual modes propagating in overmoded waveguide has been described. The use of fixed electric field probes mounted in enlarged waveguide provides for increased accuracy and permits total multimode power measurements using the technique presented by Taub [1].

By employing phase-sensitive detection, simple voltage measurements are required at only a single transverse plane. The data processing to determine the relative amplitude and phase of each mode can be carried out manually. A computation table was derived which facilitates this manual data reduction.

The experimental results presented were intended to demonstrate various measurement setups that can be used to measure the performance of standard waveguide components, or specially designed components intended for use in overmoded waveguide. The successful application of the technique to obtain data of overmoded aperture illumination for use with antenna pattern prediction methods was presented.

Acknowledgment

The authors would like to thank O. Hinckelmann, formerly of AIL, for contributing some of the basic ideas for this mode measurement technique, and the personnel of the Electromagnetic Vulnerability Laboratory, Rome Air Development Center, Griffiss AFB, N. Y., for their assistance and continued support of these programs.

References

[1] J. J. Taub, "A new technique for multimode power measurement," *IRE Trans. on Microwave Theory and Techniques*, vol. MTT-10, pp. 496–505, November 1962.
[2] M. P. Forrer and K. Tomiyasu, "Determination of high-order propagating modes in waveguide systems," *J. Appl. Phys.*, vol. 29, pp. 1040–1045, July 1958.
[3] D. J. Lewis, "Mode couplers and multimode measurement techniques," *IRE Trans. on Microwave Theory and Techniques*, vol. MTT-7, pp. 110–116, January 1959.
[4] V. G. Price, "Measurement of harmonic power generated by microwave transmitters," *IRE Trans. on Microwave Theory and Techniques*, vol. MTT-7, pp. 116–120, January 1959.
[5] E. D. Sharp and E. M. T. Jones, "A sampling technique for the measurement of multimode harmonic power," *Third Nat'l. Symp. on Radio Frequency Interference*, pp. 39–41, June 12, 1961.
[6] L. N. Engel and F. J. Morris, "Techniques of multimodal analysis in waveguides employing a semi-infinite slab of mercury," Rome Air Development Center, Griffiss AFB, N. Y., Rept. RADC-TDR-64-248, July 1964.
[7] Y. Klinger, "The measurement of spurious modes in overmoded waveguides," *Proc. IEE (London)*, vol. 106B, pp. 89–93, September 1959.
[8] D. S. Levinson and N. Worontzoff, "Use of AIL multimode power measuring technique to measure spurious emission profile of operational AN/FPS-6 height-finding radar," *Field Trip Report*, Airborne Instruments Laboratory, Deer Park, N. Y., January 1965.
[9] O. F. Hinckelmann, R. L. Sleven, and L. F. Moses, "Instrumentation for the measurement of spurious emissions in waveguide," *IRE Trans. on Electromagnetic Compatibility*, vol. EMC-6, pp. 30–37, October 1964.
[10] D. S. Levinson, "Transmission line measurement techniques," Rome Air Development Center, Griffiss AFB, N. Y., Rept. RADC-TDR-65-187, April 1965.
[11] S. Krishnan, "Diode phase detector," *Electronics*, vol. 36, pp. 45–50, February 1959.
[12] G. C. Southworth, *Principles and Applications of Waveguide Transmission*. Princeton, N. J.: Van Nostrand, 1959, p. 356.
[13] O. M. Salati and D. J. Lewis, "Interference studies," Rome Air Development Center, Griffiss AFB, N. Y., Rept. RADC-TDR-61-11, January 1961.
[14] L. B. Felsen and N. Marcuvitz, "Modal analysis and synthesis of electromagnetic fields," Microwave Research Instr. P.I.B., Rept. R-446-55(a) and (b), February 1956.